

ASCA detection of the Fe K edge in the spectrum of the Seyfert 2 galaxy IRAS 04575-7537: a sign of a complex absorber

C. Vignali¹, A. Comastri², G.M. Stirpe², M. Cappi^{3,4}, G.G.C. Palumbo^{1,3}, M. Matsuoka⁴, G. Malaguti³, and L. Bassani³

¹ Dipartimento di Astronomia, Università di Bologna, Via Zamboni 33, I-40126 Bologna, Italy

² Osservatorio Astronomico di Bologna, Via Zamboni 33, I-40126 Bologna, Italy

³ Istituto per le Tecnologie e Studio Radiazioni Extraterrestri ITeSRE/CNR, via Gobetti 101, I-40129 Bologna, Italy

⁴ The Institute of Physical and Chemical Research (*RIKEN*), 2-1, Hirosawa, Wako, Saitama, 351-01, Japan

Received / Accepted

Abstract. ASCA X-ray spectral analysis of the Seyfert 2 galaxy IRAS 04575–7537 is presented. The main result is the presence of a significant iron edge at a rest energy of $7.13_{-0.16}^{+0.21}$ keV. The spectrum is flat ($\Gamma \sim 1.5$) with a substantial absorption $N_{\text{H}} \sim 10^{22} \text{ cm}^{-2}$ and does not require any reflection component. There is also evidence of a narrow Fe K α emission line, whose rest energy ($E = 6.35_{-0.03}^{+0.08}$ keV) and equivalent width ($EW \simeq 130 \pm 50$ eV) suggest that the line originates from thick and cold matter. The intensity of the line and, in particular, the depth of the iron edge are too strong to be explained by simple transmission through the measured absorption column density. This strongly suggests that a model more complex than a single absorbed power law is needed. We propose an absorption model that we call “leaky-total absorber” which can explain the spectrum flatness, the iron emission line and the edge absorption feature and has also the advantage of having a straightforward physical interpretation in the framework of Unified models. In this model a thick absorber ($N_{\text{H}} \sim 10^{23} \text{ cm}^{-2}$), possibly associated with broad line region (BLR) clouds, partially ($\sim 36\%$) covers the source continuum with Γ fixed to 1.9 as observed in Sey 1 galaxies. The escaping radiation is then absorbed by a column density $N_{\text{H}} \sim 10^{22} \text{ cm}^{-2}$, which can be attributed to the torus, seen through its rim.

Key words: X-rays: galaxies – Galaxies: active – Galaxies: Seyfert – Galaxies: individual: IRAS 04575–7537 – Galaxies: emission lines

1. Introduction

The main idea behind the Unification models for Active Galactic Nuclei (see Antonucci 1993 and references therein for a review) is that orientation plays a significant and decisive role in Seyfert classification. In terms of our current understanding of AGNs, the central engine is probably a massive black hole, surrounded by an accretion disk and fast-moving clouds, responsible for the production of strong gravitationally and Doppler-broadened lines, completely covered by a molecular torus. More distant uncovered clouds are, on the contrary, the origin of the narrow lines. Studies of the X-ray spectra of Seyfert 2 galaxies (Awaki & Koyama 1993) have revealed the presence of highly obscured nuclei with power law spectra and Fe K α lines similar to Seyfert 1 objects providing further support to the popular Unification models for AGNs. If the orientation is such that the line of sight intercepts the torus (Krolik & Begelman 1986), the Optical/UV radiation including the BLR emission as well as soft X-rays from the nucleus are blocked and the source, visible at these wavelengths in scattered light, is classified as a type 2. The scattering medium (Krolik & Kallman 1987), whose physical state is unfortunately still poorly known, is likely to be a warm plasma located along the torus axis.

With respect to the hard X-ray emission, the spectral index distribution of Seyfert 2’s should be the same as for Seyfert 1’s. However this seems not to be the case, since discrepancies from the Unification scenario have been reported. In fact, the re-analysis of a sample of 15 Seyfert 2 galaxies observed by GINGA (Smith & Done 1996) has indicated that the spectral slope of about half of them is significantly flatter ($\Gamma \sim 1.5$) than the mean value found for Seyfert 1 ($\Gamma \sim 1.9$ -2.0, Nandra & Pounds 1994; Gondek et al. 1996). At least 4 of these sources are incompatible with the steep Seyfert 1 slope, even with the addition to the primary spectrum of a strong reflection component. Moreover, Awaki (1991) has pointed out that a small sub-

Send offprint requests to: C. Vignali

Correspondence to: l.vignali@astbo3.bo.astro.it

sample of IRAS selected Seyfert 2 galaxies shows no evidence of any obscuring medium ($N_{\text{H}} < 10^{22} \text{ cm}^{-2}$) and is well described by a rather steep continuum with no reflection component. On the basis of these results there seems to be growing evidence in favour of a more complex scheme for the X-ray emission of Seyfert 2 galaxies. To further investigate some of these issues we have observed with ASCA one of the galaxies in the Awaki (1991) sub-sample.

IRAS 04575–7537 is associated with a rather bright ($m_V = 14.5$) barred spiral galaxy ($z = 0.0184$) and is characterized by a strong infrared emission, $F_{\text{FIR}(40-120\mu\text{m})} \simeq 4.2 \times 10^{-11} \text{ erg cm}^{-2} \text{ s}^{-1}$, corresponding to a $L_{\text{FIR}} \simeq 6.2 \times 10^{43} \text{ erg s}^{-1}$ (Ward & Morris 1984; Boller et al. 1992), which dominates over the optical emission (de Grijp et al. 1987, 1992). First detected in the X-ray band by the HEAO1 satellite (Wood et al. 1984), it was then observed by the GINGA/LAC (Awaki 1991; Smith & Done 1996). It revealed a steep ($\Gamma \simeq 2.1 \pm 0.2$), mildly absorbed ($N_{\text{H}} \simeq 1.2_{-0.4}^{+0.7} \times 10^{22} \text{ cm}^{-2}$) continuum, plus an iron line ($\text{EW} \simeq 260 \pm 110 \text{ eV}$). It also appears as a bright X-ray source in the ROSAT All-Sky Survey (Moran et al. 1996), having a soft (0.1–2.4 keV) X-ray luminosity of about $10^{43} \text{ erg s}^{-1}$, a typical value for a Seyfert 1 nucleus. Here we present an ASCA spectrum that allows a more detailed analysis of the 0.5–10 keV spectrum of this source.

Given that the optical classification of IRAS 04575–7537 as a Seyfert 2 is based on a low signal-to-noise spectrum (Kirhakos & Steiner 1990; de Grijp et al. 1992), we have also performed an optical observation, which is discussed in Sect. 2. Section 3 describes the ASCA observation and data reduction. Section 4 presents the X-ray timing and spectral analysis. The results are described in Sect. 5 and summarized in Sect. 6.

Throughout the paper a Friedmann cosmology with a Hubble constant $H_0 = 50 \text{ Km s}^{-1} \text{ Mpc}^{-1}$ and a deceleration parameter $q_0 = 0$ are assumed.

2. Optical spectrum and classification

An optical spectrum of IRAS 04575–7537 was obtained in photometric conditions at the ESO 1.5m telescope on 1996 October 1, with a slit width of 2 arcsec, at a resolution of 4.6 \AA . The integration time was 30 minutes. Standard reduction and calibration techniques were used, and the resulting spectrum is shown in Fig. 1.

The spectrum presents several strong emission lines, none of which has a broad component, thus ruling out the Seyfert 1 galaxy type. The fluxes of the main emission lines were obtained by fitting them with single Gaussians and integrating the latter. The fluxes are listed in Table 1. As shown by Baldwin et al. (1981) and Veilleux & Osterbrock (1987), ratios between fluxes of close lines can be used to determine whether a narrow emission line region is

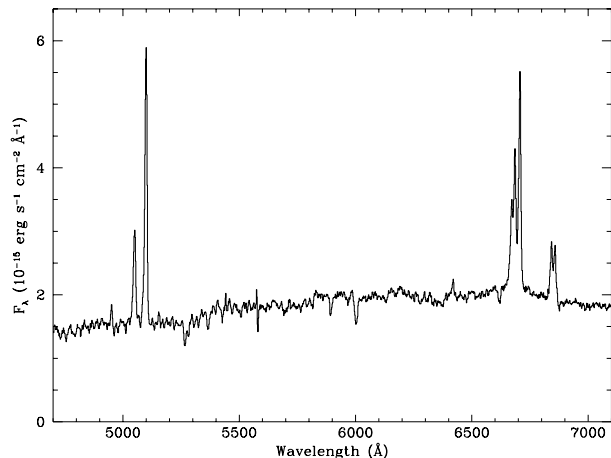


Fig. 1. The optical spectrum of IRAS 04575–7537, in the rest system of the observer ($z = 0.0184$)

Table 1. Characteristics of the main optical lines

Line	Total flux ($10^{-14} \text{ erg s}^{-1} \text{ cm}^{-2}$)	EW (Angstrom)
H β	0.2	2
[O III] λ 4959	1.7	10
[O III] λ 5007	5.0	33
[O I] λ 6300	0.2	1
[N II] λ 6548	1.6	7
H α	2.5	12
[N II] λ 6584	3.9	18
[S II] λ 6717	1.0	6
[S II] λ 6731	1.0	5

most likely to be photoionized by hot stars (as in starburst galaxies) or by an active nucleus (as in Seyfert 2 galaxies or in LINERS). In the [O III] λ 5007/H β vs. [N II] λ 6584/H α diagnostic diagram proposed by the above cited authors, the flux ratios of IRAS 04575–7537 (20 and 1.5 respectively) place it well in the Seyfert 2 domain. The same occurs in the [O III] λ 5007/H β vs. [O I] λ 6300/H α and [O III] λ 5007/H β vs. [S II] λ 6717 + λ 6731/H α diagrams. The largest FWHM of the emission lines ($\sim 500 \text{ km s}^{-1}$) is also typical for Seyfert 2 galaxies. We therefore confirm the Seyfert 2 classification and exclude a strong starburst component.

3. ASCA data reduction

The observation reported here was carried out by the *Advanced Satellite for Cosmology and Astrophysics* (ASCA) during the period 1996 November 4–5. The satellite contains four sets of conical foil mirrors that focus X-rays into four instruments covering the 0.4–10 keV energy band (Tanaka et al. 1994): two solid-state spectrometers (SIS,

Gendreau 1995), each consisting of 4 CCD chips yielding $\sim 2\%$ nominal energy resolution (FWHM) at 6 keV, and two gas imaging spectrometers (GIS, Makishima et al. 1996) with $\sim 8\%$ energy resolution at 6 keV. The SIS data were obtained in 1-CCD readout mode, whereby only 1 CCD chip is exposed on each SIS with the target at the nominal pointing position. The FAINT mode data were converted into BRIGHT2 mode data (corrected for dark-frame error and for echo effect), in order to minimize the effect of slight changes in the energy scale on the results. The following selection criteria were applied to the data: the spacecraft had to be outside the South Atlantic Anomaly; the elevation angle above the Earth limb greater than 5° ; the bright Earth angle, i.e. the angle above the Sun-illuminated Earth's limb, greater than 15° ; the magnetic cut-off rigidity (COR) greater than 6 GeV c^{-1} for SIS and 7 GeV c^{-1} for GIS. “Hot” and flickering pixels were removed from the SIS using an algorithm that excludes pixels showing count rates outside the expected Poissonian distribution estimated from neighbouring pixels; also rise-time rejection was applied to exclude particle events for the GIS data. SIS grades 0, 2, 3, 4 and 6 were selected for the analysis. The introduction of grade 6 gives both an improvement in the source photon number, especially at energies above 5–6 keV (Weaver et al. 1997), and better constraints to the spectral parameters. Moreover, the results are in agreement with the ones obtained with a more “standard” reduction without the introduction of the grade 6. The spectra were extracted from box regions of about $8' \times 5'$ for the SIS and from circular regions of radius $\sim 6'$ for the GIS, both centered on the source. Background SIS spectra were taken from box source-free regions in the same chip which contained the source, while for the GIS a circular background region was used from a position near the source and at the same distance from the optical axis.

After removing a short period of unstable pointing prior to target acquisition, a total of ~ 34 Ks/SIS and 35 Ks/GIS were available for the spectral analysis. The source count rates (in units of counts s^{-1}) are 0.191 ± 0.003 and 0.157 ± 0.002 in the 0.4–10 keV band for SIS0 and SIS1, respectively, and 0.151 ± 0.002 and 0.153 ± 0.003 in the 0.7–10 keV band for GIS2 and GIS3, respectively. Data preparation and spectral analysis were performed using version 1.3 of the XSELECT package and version 9.01 of XSPEC (Arnaud et al. 1996).

4. ASCA analysis and results

4.1. Timing analysis

Figure 2 shows the 0.5–10 keV source+background (top) and background (bottom) light curves binned at 2800 s, which indicates that the background level (2.3×10^{-2} counts s^{-1}) was stable during the ASCA pointing. The

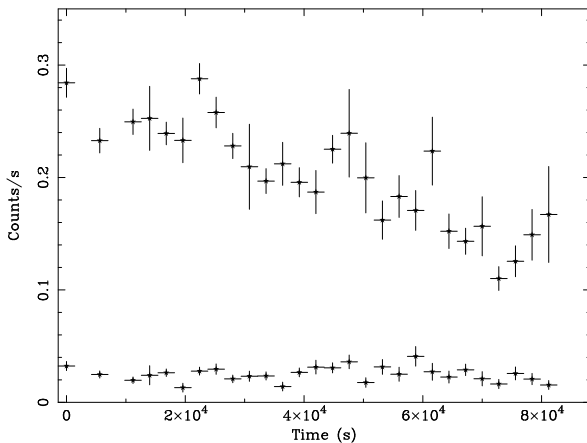


Fig. 2. IRAS 04575-7537 source+background light curve (top) and background light curve (bottom) in the 0.5–10 keV energy range. Bin interval is 2800 s

data are taken from SIS0, since no significant differences have been found among SIS and GIS. Flux variability with a doubling time of about 50 000 s (thus constraining the dimensions of the emitting region to be of the order of 10^{15} cm) and variations of the order of 35% on shorter time scales of about 20 000 s have been detected. The amplitude of the variability and the characteristic time-scales found for IRAS 04575–7537 are typical of Seyfert 1 galaxies (Mushotzky et al. 1993). It should be noted that no clear evidence of variability has been found in the soft (0.5–1.0 keV) light curve, whereas it is clearly present in the hard (2–10 keV) light curve. In order to look for spectral variability, a high- and a low-state spectrum were extracted, with about 0.2 counts s^{-1} as the dividing line between the two states. Because of the rather poor statistics of the low-state spectrum, no conclusive information about spectral variability can be obtained. As a further check, the dividing line between the two states was chosen in such a way that the counting statistics was the same for both states. The derived high-state spectrum seems to be steeper than the low-state one, similar to what is observed in Seyfert 1 galaxies (Mushotzky et al. 1993). However, this result is only marginally significant and, therefore, it will not be considered any further. No significant flux variability has been detected between ASCA and GINGA observations on a time scale of 6 years.

4.2. Spectral analysis

GIS and SIS spectra were binned with more than 20 counts per bin in order to apply the χ^2 statistics. In the following, errors are given at 90% of confidence for one interesting parameter ($\Delta\chi^2 = 2.71$, Avni 1976). At first, a simple absorbed power law model was fitted to the data of

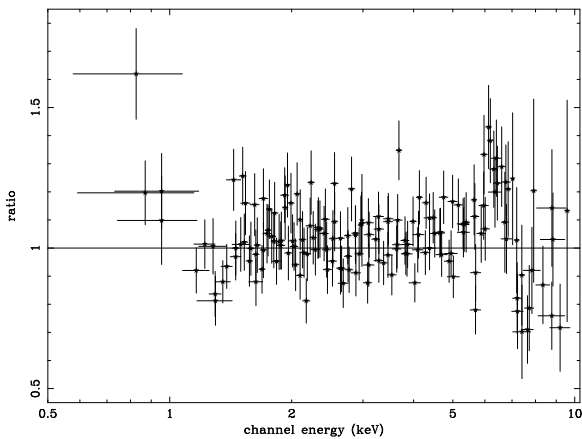


Fig. 3. Plot of the data/model ratio. The presence of an iron line + edge is suggested by the residuals in the power law plus absorption model. A soft component is also evident below ~ 1 keV

each SIS/GIS detector. Since the results were all in agreement, within the errors, and the residuals from the fit were very similar, the two SIS and the two GIS spectra were added together. In the analysis described below the data were, therefore, fitted simultaneously using the same model, with the relative normalizations of SIS and GIS left free to vary. The best-fit parameters are given in Table 2.

A simple power law continuum plus photoelectric absorption from cold material with cosmic abundances given by Anders & Grevesse (1989) and cross sections derived from Balucinska-Church & McCammon (1992) does not provide an adequate fit to the data. The plot of the data to model ratio (Fig. 3) clearly reveals the presence of an iron line emission at about 6.4 keV plus an absorption edge at about 7 keV, as well as excess emission below 1 keV. Given the poor statistical quality of the data below 1 keV, the following will mainly focus on the X-ray properties of IRAS 04575–7537 at energies > 1 keV.

Besides the spectral features at 6–7 keV, a single absorbed ($N_{\text{H}} \simeq 10^{22} \text{ cm}^{-2}$) power law gives a flat slope, $\Gamma \simeq 1.4$ –1.5 (Fig. 4), which is significantly different from the GINGA slope $\Gamma \simeq 2.1 \pm 0.2$ (Smith & Done 1996). The steeper GINGA spectrum can be, at least partially, explained in terms of contamination of the GINGA data by a nearby K III peculiar star, which is at a distance of about $18'$ in the GIS field of view from IRAS 04575–7537, has a 2–10 keV flux of $\sim 7 \times 10^{-12} \text{ erg cm}^{-2} \text{ s}^{-1}$ (to be compared with the Seyfert 2 flux of $1.2 \times 10^{-11} \text{ erg cm}^{-2} \text{ s}^{-1}$) and has a steep power law continuum with $\Gamma = 2.7 \pm 0.2$.

A net improvement in the spectral fit is achieved after the addition of a gaussian line at 6.4 keV ($\Delta\chi^2 = 30$). If the gaussian width is kept narrow ($\sigma = 0 \text{ eV}$) and the central energy and intensity of the line are left free

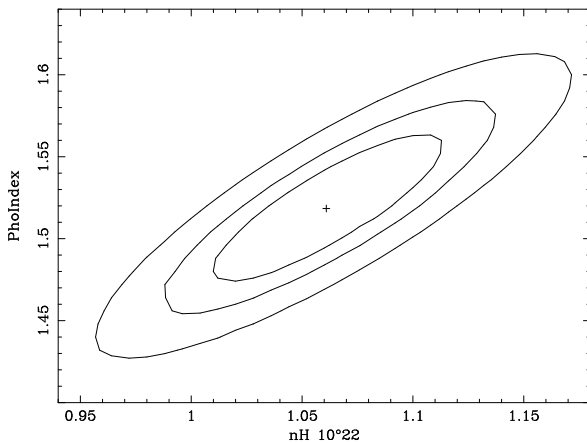


Fig. 4. Plot of the confidence contours for the spectral slope and absorption column density (second line of Table 2). The contours represent 68, 90 and 99 % confidence intervals

to vary, the best fit values (rest frame) are $E = 6.35^{+0.08}_{-0.03}$ keV (almost neutral) and $EW = 165 \pm 49 \text{ eV}$. The upper limit to the line width is about 100 eV, which is consistent with the SIS energy resolution at the time the observation was carried out. The data to model ratio (Fig. 3) clearly suggests an absorption feature above 7 keV. Since there is no instrumental level of uncertainty larger than 10% around this energy and the background spectra are taken from source-free regions nearby IRAS 04575–7537, one can confidently assume that this feature is a real physical structure in the data. The addition of an iron edge at $E = 7.13^{+0.21}_{-0.16}$ keV results to be significant at $> 99.9\%$ level ($\Delta\chi^2 = 18$ with two more degrees of freedom), according to an F-test. Iron K edges have been recently detected by ASCA in some other Seyfert 2 galaxies (Turner et al. 1997). The values of both the edge energy and absorption depth are similar to the present ones.

Regardless of the model used to fit the 0.5–10 keV spectrum, the photon index remains flat ($\Gamma = 1.5 \pm 0.05$, Fig. 4) and incompatible with the Seyfert 1s value of 1.9 ± 0.1 (Nandra & Pounds 1994; Nandra et al. 1997). The addition of a reflection component brings no improvement in the spectral fitting (Table 2, lines 4 and 5), even if the photon index is forced to be steep ($\Gamma = 1.9$). In a similar way, a warm absorber model applied to the hard component is not a satisfactory explanation for IRAS 04575–7537 complex spectrum, the absorption edge being still highly significant.

5. Discussion

Table 2. Results of spectral fits.

τ_{edge} is the absorption depth of the iron edge, \mathfrak{R} represents the reflection parameter, where $\mathfrak{R} = 1$ for isotropic illumination

Γ_{soft}	Γ_{hard}	N_{H} (10^{22} cm^{-2})	E_{line} (keV)	EW (eV)	E_{edge} (keV)	τ_{edge}	\mathfrak{R}	χ^2/dof
...	$1.47^{+0.05}_{-0.04}$	1.03 ± 0.06	867/814
...	1.52 ± 0.05	1.06 ± 0.06	$6.35^{+0.07}_{-0.03}$	165 ± 49	837/812
...	1.43 ± 0.06	$0.99^{+0.07}_{-0.06}$	$6.35^{+0.08}_{-0.03}$	129^{+46}_{-47}	$7.13^{+0.21}_{-0.16}$	$0.33^{+0.14}_{-0.13}$...	819/810
...	$1.48^{+0.21}_{-0.10}$	$1.01^{+0.13}_{-0.07}$	$6.35^{+0.09}_{-0.04}$	115^{+62}_{-61}	7.13 ± 0.18	$0.34^{+0.14}_{-0.13}$	< 3.24	819/809
...	1.90 fr.	$1.24^{+0.05}_{-0.04}$	$6.35^{+0.10}_{-0.08}$	72^{+53}_{-46}	$7.05^{+0.19}_{-0.17}$	$0.32^{+0.14}_{-0.13}$	$6.46^{+1.05}_{-1.15}$	830/810
$1.49^{+0.07}_{-0.06}$	$\Gamma_{\text{s}} = \Gamma_{\text{h}}$	1.05 ± 0.10	$6.35^{+0.08}_{-0.03}$	142^{+49}_{-50}	$7.14^{+0.25}_{-0.17}$	0.29 ± 0.14	...	809/809

5.1. X-ray continuum properties

The intrinsic hard X-ray luminosity of IRAS 04575–7537 ($L_{\text{X}} \simeq 2 \times 10^{43} \text{ erg s}^{-1}$ in the 2–10 keV energy range) and the variability suggest the presence of a Seyfert 1 nucleus. The optical spectrum does not reveal any broad component, confirming that absorption effects play an important role. The best fit spectral slope, $\Gamma \sim 1.5$, is rather flat and similar to the value found in other flat-spectrum Seyfert 2 galaxies (Smith & Done 1996; Cappi et al. 1996; Iwasawa et al. 1997), thus increasing the number of Seyfert 2 galaxies with flat spectra that are apparently inconsistent with the predictions of the Unified models. A simple extrapolation of the X-ray spectral slope up to 100 keV gives a 2–100 keV luminosity of about $6.0 \times 10^{43} \text{ erg s}^{-1}$, in excellent agreement with the far-infrared (40–120 μm) luminosity ($L_{\text{FIR}} \simeq 6.2 \times 10^{43} \text{ erg s}^{-1}$, Boller et al. 1992). This seems to confirm the validity of a reprocessing scenario, in which most of the optical-UV-X-ray radiation emitted by the central source is intercepted by the torus, which reemits a fraction of this energy in the infrared band (Krolik & Lepp 1989; Pier & Krolik 1992).

5.2. Origin of the iron line and edge

Assuming the iron cross section given by Leahy & Creighton (1993), the measured absorption depth $\tau = 0.33^{+0.14}_{-0.13}$ implies an equivalent hydrogen column density $N_{\text{H}} = 2\text{--}4 \times 10^{23} \text{ cm}^{-2}$, which is much larger than the value obtained from the spectral analysis ($N_{\text{H}} \sim 10^{22} \text{ cm}^{-2}$). The lack of a reflection component seems to indicate that the iron line takes its origin through transmission, but both the observed FeK α edge depth and line EW are found to be inconsistent with the measured absorption column density unless an unrealistic factor ~ 10 iron overabundance is assumed.

The complex picture that derives from data analysis could be explained in a way similar to the model proposed by Hayashi et al. (1996) for the Narrow Emission Line Galaxy (NELG) NGC 2110 and previously by Weaver et al. (1994) for NGC 4151. This requires the presence of a

dual-absorber model, in which the iron features revealed by ASCA originate in a two-phase cold matter. Such a model has been successfully fitted to the IRAS 04575–7537 spectrum and the results are reported in Table 3. Cold material with a column density of the order of 10^{23} cm^{-2} partially covers the nucleus, with an average covering factor value of about 36 %, and is responsible for a substantial part of the iron line and edge features. An additional component with $N_{\text{H}} \sim 10^{22} \text{ cm}^{-2}$, totally covering the central source, is responsible for the optical and soft X-ray absorption and provides a further contribution to the X-ray features. Since the intrinsic luminosity ($L_{\text{X}} \sim 2 \times 10^{43} \text{ erg s}^{-1}$) is typical of a Seyfert 1 nucleus, the underlying X-ray continuum is parameterized by a power law with spectral index 1.9 (Nandra & Pounds 1994; Nandra et al. 1997). Following the calculations of Leahy & Creighton (1993, see their Fig. 2) the measured absorbing column density predicts a FeK α line EW and edge depth consistent with the measured values, once they are scaled for the covering fraction obtained from the spectral fitting. As a proof of this result, the addition of a FeK α edge is no longer required by the data, since a column density of the order of 10^{23} cm^{-2} can account for the iron edge. Even if this model, that we call “leaky-total absorber”, provides a greater χ^2 (Table 3) than the previous absorbed power law plus iron edge fit (Table 2, line 3), it is interesting to note that it explains the iron features and offers a straightforward physical interpretation consistent with the predictions of Unified models as well. The partially ($\sim 36\%$) covering material ($N_{\text{H}} \sim 10^{23} \text{ cm}^{-2}$) could indeed be associated either with the BLR clouds or with blobs, under the assumption that they are small if compared with both the size of the X-ray source and the radius of their distribution. This may be possible in a context of confinement by strong equipartition magnetic fields (Rees 1987) or by radiation pressure induced by the primary source (Celotti et al. 1992). Also the line width ($\sigma \leq 100 \text{ eV}$, corresponding to $\sim a \text{ few} \times 10^3 \text{ Km s}^{-1}$) is consistent with typical values for BLR clouds (Ghisellini et al. 1994). Moreover the BLR are known from optical observations (Kwan & Krolik 1981) to have column densities just of the order of

Table 3. “Leaky-total absorber” model. N_{H_1} is the column density of the totally covering material, while N_{H_2} represents the absorption due to the partially covering one

Γ	N_{H_1} (10^{22} cm^{-2})	E_{line} (keV)	EW (eV)	N_{H_2} (10^{22} cm^{-2})	Cvr Fract (%)	χ^2/dof
1.9 (f)	$1.22^{+0.05}_{-0.06}$	$6.35^{+0.08}_{-0.03}$	158^{+47}_{-48}	$10.9^{+4.20}_{-3.37}$	$36.1^{+3.5}_{-3.8}$	832/811

those observed in the X-ray spectrum. The totally covering absorber could be associated with the obscuring torus that hides the active nucleus. The derived column density requires that either the torus is intrinsically optically thin or we are looking through its rim, which is consistent with the observed source variability.

An alternative, but similarly speculative, explanation of IRAS 04575–7537 geometry and X-ray emission introduces a more complex configuration for the torus (Maiolino & Rieke 1995). If the gravitational potential is dominated by nuclear mass, as in the case of AGNs, then the Roche limit requires that the inner parts of the torus are tidally disrupted when they approach a distance (Lang 1980)

$$R(\text{pc}) = 2.5 [M_{\text{BH}}(M_{\odot}) / \rho(\text{cm}^{-3})]^{1/3}$$

Thus, when a typical molecular cloud in a Seyfert galaxy moves within this radius, it will be destroyed by the nuclear black hole gravitational potential. This can explain the partially covering absorber, whereas the outer parts of the torus remain quite homogeneous and can be associated with the totally covering absorber.

5.3. The soft excess

In order to model the soft X-ray emission, the 0.4–10 keV spectrum was fitted adding to the high-energy best-fit spectrum a soft component, either a thermal plasma or a power law model, and fixing the absorption of the soft component at the Galactic value ($N_{\text{Hgal}} = 9 \times 10^{20} \text{ cm}^{-2}$, Dickey & Lockman 1990). Due to the low number of source counts below 1 keV, it has not been possible to discriminate between a thermal component or a scattering power law model for the soft X-ray excess from the present data. The 0.5–4.5 keV X-ray luminosity derived from the thermal model is $\sim 4.3 \times 10^{41} \text{ erg s}^{-1}$ and is likely to be associated to hot gas in the host galaxy. This value results to be more than an order of magnitude larger than the one ($L_{\text{X}} \sim 3.8 \times 10^{40} \text{ erg s}^{-1}$) expected for bright infrared normal and starburst galaxies, assuming the far-infrared/X-ray luminosity correlation of David et al. (1992). This suggests that IRAS 04575–7537 soft X-ray excess is due to scattered nuclear X-ray emission. In this context, a scattering model gives a rather good description of the data (Table 2, line 6), and provides a fraction of $\sim 3\%$ of scattered emission. Archival ROSAT PSPC data have also been analyzed. The source is about

18' from the center of the field of view. The spectral analysis confirms that the spectrum is highly absorbed ($N_{\text{H}} \sim 10^{22} \text{ cm}^{-2}$), but the existence of a soft excess appears marginal, since the high galactic column density hampers a spectral study below $\sim 0.7 \text{ keV}$. It should be noted that the high soft X-ray luminosity (about $10^{43} \text{ erg s}^{-1}$) found by Moran et al. (1996) must be ascribed to the ROSAT 1–2 keV flux, where the hard luminous X-ray component is already significant.

6. Conclusions

The ASCA observation of the Sey 2 galaxy IRAS 04575–7537 has revealed a complex spectrum. Relevant points may be summarized as follows:

1. Hard X-ray variability, of a factor > 2 over a time scale of about $5 \times 10^4 \text{ s}$, has been detected, without a significant evidence of spectral variability.
2. The hard ($E > 1 \text{ keV}$) X-ray continuum is well described by an absorbed power law model, whose flat spectral slope ($\Gamma \sim 1.5$) cannot be accounted for by a strong reflection component on a steeper primary power law, suggesting a possible inconsistency with the predictions of the Unified models.
3. Iron $K\alpha$ absorption edge and emission line have been clearly detected. Both of them are consistent with neutral or mildly ionized (less than Fe XVII) iron, but are too strong to be explained by transmission through the observed absorption column density ($N_{\text{H}} \sim 10^{22} \text{ cm}^{-2}$).
4. Excess X-ray emission below 1 keV is detected, but the present data do not allow to discriminate between a thermal and a scattering model.
5. The whole observation can be explained assuming a model, called “leaky-total absorber”, which consists of a dual-absorber configuration, where the underlying continuum is parameterized to be that of a Seyfert 1 ($\Gamma = 1.9$). A partially ($\sim 36\%$) covering material, either BLR clouds or the inner, disrupted parts of the torus, surrounds the source and gives rise to an absorption of about 10^{23} cm^{-2} . This material is considered to be responsible for the iron line and edge features. Moreover, the totally covering matter, probably associated with the molecular torus (or the outer parts of

it), produces the optical and the soft X-ray absorption ($N_{\text{H}} \sim 10^{22} \text{ cm}^{-2}$). This model explains the observed spectral features, has the advantage to have a straightforward physical interpretation in the framework of Unified models and provides a solution of the apparent puzzle of points 2 and 3.

Acknowledgements. We thank all the members of the ASCA team who operate the satellite and maintain the software and database. This work has made use of the NASA/IPAC Extragalactic Database (NED) which is operated by the Jet Propulsion Laboratory, Caltech, under contract with the National Aeronautics and Space Administration, of data obtained through the High Energy Astrophysics Science Archive Research Center Online Service, provided by the Goddard Space Flight Center and of the Simbad database, operated at CDS, Strasbourg, France. Financial support from Italian Space Agency under the contract ARS-96-70 and MURST is acknowledged by CV, AC, MC and GGCP. The authors are grateful to R. Pazzaglia for the helpful suggestions about the “leaky-total absorber” model. Moreover, CV wishes to thank all those people who encouraged him to write this paper.

References

- Anders E., Grevesse N., 1989, *Geochimica et Cosmochimica Acta* 53, 197
- Antonucci R.R.J., 1993, *ARA&A* 31, 473
- Arnaud K.A., 1996, in: *Astronomical Data Analysis Software and Systems V*, Jacoby G., Barnes J. (eds.), ASP Conf. Series, vol. 101, 17
- Avni Y., 1976, *ApJ* 210, 642
- Awaki H., 1991, PhD Thesis, University of Nagoya
- Awaki H., Koyama K., 1993, *Adv. Space Res.* vol. 13, n. 12, p. 12 (221)
- Baldwin J.A., Phillips M.M., Terlevich R., 1981, *PASP* 93, 5
- Balucinska-Church M., McCammon D., 1992, *ApJ* 400, 699
- Boller Th., Meurs E.J.A., Brinkmann W., et al., *A&A* 261, 57
- Cappi M., Mihara T., Matsuoka M., et al., 1996, *ApJ* 456, 141
- Celotti A., Fabian A.C., Rees M.J., 1992, *MNRAS* 255, 419
- David L.P., Jones C., Forman W., 1992, *ApJ* 388, 82
- de Grijp M.H.K., Miley G.K., Lub J., 1987, *A&AS* 70, 95
- de Grijp M.H.K., Keel W.C., Miley G.K., Goudfrooij P., Lub J., 1992, *A&AS* 96, 389
- Dickey J.M., Lockman F.J., 1990, *ARA&A* 28, 215
- Gendreau K., 1995, PhD Thesis, Massachusetts Institute of Technology
- Ghisellini G., Haardt F., Matt G., 1994, *MNRAS* 267, 743
- Gondek D., Zdziarski A.A., Johnson W.N., et al., 1996, *MNRAS* 282, 646
- Hayashi I., Koyama K., Awaki H., Ueno S., Yamauchi S., 1996, *PASJ* 48, 219
- Iwasawa K., Fabian A.C., Brandt W.N., Crawford C.S., Almaini O., 1997, *MNRAS* 291, L17
- Kirhakos S.D., Steiner J.E., 1990, *AJ* 90, 1722
- Krolik J.H., Begelman M.C., 1986, *ApJ* 308, L55
- Krolik J.H., Kallman T.R., 1987, *ApJ* 320, L5
- Krolik J.H., Lepp S., 1989, *ApJ* 347, 179
- Kwan J., Krolik J.H., 1981, *ApJ* 250, 478
- Lang K.R., 1980, in: *Astrophysical Formulae*, p. 280
- Leahy D.A., Creighton J., 1993, *MNRAS* 263, 314
- Makishima K., Tashiro M., Ebisawa K., et al., 1996, *PASJ* 48, 171
- Maiolino R., Rieke G.H., 1995, *ApJ* 454, 95
- Moran E.C., Halpern J.P., Helfand D.J., 1996, *ApJS* 106, 341
- Mushotzky R.F., Done C., Pounds K.A., 1993, *ARA&A* 31, 717
- Nandra K., Pounds K.A., 1994, *MNRAS* 268, 405
- Nandra K., George I.M., Mushotzky R.F., Turner T.J., Yaqoob T., 1997, *ApJ* 477, 602
- Pier E.A., Krolik J.H., 1992, *ApJ* 401, 99
- Rees M.J., 1987, *MNRAS* 228, 47p
- Smith D.A., Done C., 1996, *MNRAS* 280, 355
- Tanaka Y., Inoue H., Holt S.S., 1994, *PASJ* 46, L37
- Turner T.J., George I.M., Nandra K., Mushotzky R.F., 1997, *ApJS* 113, 23
- Veilleux S., Osterbrock D.E., 1987, *ApJS* 63, 295
- Ward M.J., Morris S.L., 1984, *MNRAS* 207, 867
- Weaver K.A., Yaqoob T., Holt S.S., et al., 1994, *ApJ* 436, L27
- Weaver K.A., Yaqoob T., Mushotzky R.F., et al., 1997, *ApJ* 474, 675
- Wood K.S., Meekins J.F., Yentis D.J., et al., 1984, *ApJS* 56, 507